Weight Estimation by Dynamic Data Acquisition

Sabag, Matthew
Section 3458 06/21/2026

***Abstract*—The objective of this experiment was to evaluate and analyze different methods of determining the weight of a liquid-filled container at distinct levels of fill. To complete this experiment, a quarter Wheatstone Bridge (WSB) paired with a strain gauge were connected to a 14-bit analog-to-digital converter (ADC) to acquire voltage signals. The strain gauge was carefully bonded to the fixed end of a 6061-T6 aluminum beam secured in a cantilever setup, where the sample being weighed was placed on the free-floating end. Using two separate sample windows to mitigate saturation, strain is computed through an amplified voltage (V_{amp}, gain = 900). With these recorded voltages, the weight can be derived from foundational engineering theory. The calibrated weight was determined using a calibration constant acquired from experimental measurements using four known weights, 0.9787 N, 1.9609 N, 2.9395 N, and 3.9222 N, each measured individually on a laboratory scale of uncertainty ± 0.0005 N. The results for the catalogued weights were 3.8222 ± 0.0005 N full and 0.2892 ± 0.0005 N empty (scale), 3.5756 ± 0.066 N full and 0.2414 ± 0.160 N empty (theory), and 3.7878 ± 0.070 N full and 0.2557 ± 0.151 N empty (calibrated). The six weight values agreed with each other, being only within a few tenths of a Newton apart and proving that strain-based weight estimation is viable, precise, and accurate.**

***Index Terms*—Analog-to-digital converter, calibration constant, cantilever beam, quarter Wheatstone bridge, sample window, saturation, strain gauge.**

I. Introduction

THE purpose of this experiment was to construct and calibrate a cantilever beam scale using a strain gauge as the primary transducer, and to use two methods to estimate the weight of a liquid container at various levels of fill. The strain gauge was bonded to the fixed end of a 6061-T6 aluminum beam, which was clamped in a cantilever configuration. When a load was applied at the free end of the beam, a bending moment was induced along its length, creating a surface stress and corresponding strain at the gauge location. The strain gauge captured this deformation as a change in resistance, which was converted into a differential voltage signal by a quarter Wheatstone Bridge (WSB). Because the raw bridge voltage, V_g, was too small to be reliably digitized, an inline amplifier scaled the signal to V_{amp} before it was read by a 14-bit analog-to-digital converter (ADC) within the data acquisition device (DAQ). This amplified signal was then sent to the 14-bit ADC monitored through the LabVIEW software. To prevent the voltage from clipping, or cutting off, while still maintaining good resolution, the software data collection windows had to be carefully adjusted based on the signal size. To establish how software settings affected data precision, the resolution limit of the DAQ was evaluated. The continuous voltage ranges were converted into discrete digital steps by a 14-bit ADC, where the smallest detectable change in voltage was determined by the sample window bounds (1). This hardware collected data at 50 Ks/sec for a duration of 50 ms, resulting in 2500 samples.

$$Resolution = \frac{V_{Max} - V_{Min}}{2^n - 1} \tag{1}$$

Here, V_{Max} and V_{Min} represented the upper and lower voltage bounds of the selected sample window, and n represented the 14-bit resolution depth of the hardware. This formula showed that narrowing the span between the maximum and minimum voltage bounds directly increased the measurement precision. This is done by reducing the size of each discrete digital step since there is a set number of digital steps as per the denominator, $n = 14$. With this, the smaller the difference, the smaller size of steps that were taken, and therefore a greater resolution. These resolution settings played a critical role in minimizing error and uncertainty in this experiment.

This laboratory experiment required an apparatus with sensitive and precise instruments. One of the instruments used was a strain gauge adhered to the aluminum beam and connecting wires were soldered to the leads of the strain gauge. This measured resistance (2) of the strain gauge, R, is directly proportional to the resistivity of the wire, ρ, the length of the wire, L, and inversely proportional to the cross-sectional area of the wire, A. This small change in resistance played a critical role in the microscopic electrical measurements that were collected.

$$R = \rho \frac{L}{A} \tag{2}$$

The resistance from the strain gauge was not the only resistance present. There was an additional component to the total resistance of the beam-strain gauge system. The terms (3) of the new unknown resistance, R_U, under load $\varepsilon \neq 0$, were internal resistance of strain gauge, R, under no load $\varepsilon = 0$, the measured strain, ε, and gauge factor, G_f. Shear and lateral strains may have been present in the beam under loading and have been accounted for in the gauge factor [5].

$$R_U = R + \varepsilon G_f R \tag{3}$$

It is imperative to understand the cantilever beam setup. By applying basic Statics and Mechanics of Materials principles to the diagram and respective lab apparatus, we were able to derive relevant equations that were used in calculating the strain on the beam's surface. The neutral axis runs along the length of the beam, L_0, and at exactly half the height, h. The applied load, W, is located at end of the beam where L is the distance for the moment arm and its associated force, from the middle of the strain gauge to the end of the beam. These values were used to acquire the magnitude of the induced moment.

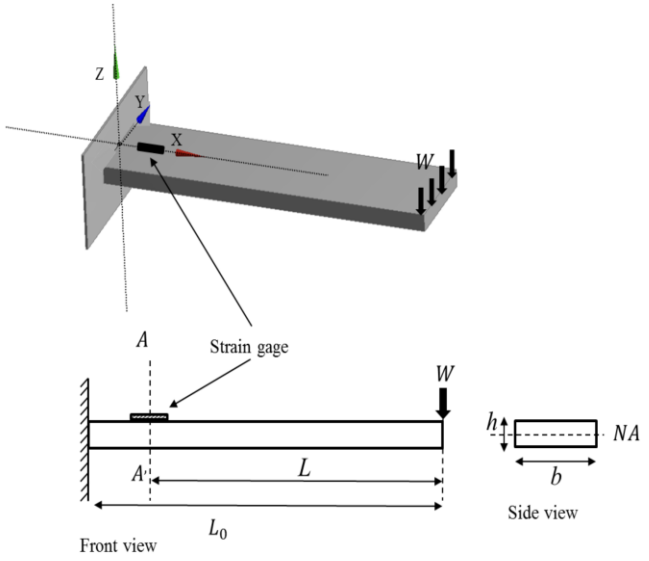

Fig. 1. A geometric view of the cantilever beam and variables dimensioned [7].

Foundational Statics and physical principles allowed us to use the moment equation (4) to evaluate the magnitude of the moment arm for the system.

$$M = L \times W \tag{4}$$

With a known height, h, and width, b, the moment of inertia, I, for a rectangular cross-section beam was determined (5).

$$I = \frac{bh^3}{12} \tag{5}$$

To find the strain at the surface, we must have first determined the distance from the point of interest to the neutral axis. As viewed from the cross-sectional area of the beam, the distance from the neutral axis to the surface is half of the height of the beam (6).

$$c = \frac{h}{2} \tag{6}$$

Using the distance from the neutral axis, c, the induced moment, M, and the moment of inertia, I, the stress along the surface of the beam, σ, was determined (7).

$$\sigma = \frac{Mc}{I} \tag{7}$$

By inserting (4-6) into (7), we can find the stress on the surface of the beam (8) from the given geometric dimensions in Fig. 1.

$$\sigma = \frac{6WL}{bh^2} \tag{8}$$

The known stress has a relationship with the material property associated with stiffness, known as Young's Modulus, E, and the strain, ε. We employed the stress/strain equation (9).

$$\sigma = E\varepsilon \tag{9}$$

After substituting in (9) into (8), we can rearrange the formula to solve for the theoretical load (10) all derived using core concepts from Statics and Mechanics of Materials.

$$W_{theory} = \frac{\varepsilon E b h^2}{6L} \tag{10}$$

The strain gauge, which functioned as a transducer that converted mechanical deflection into resistance changes, was bonded directly to the surface of the aluminum beam and directly converted the readings into measurable strain. To capture these microscopic changes, the strain gauge was wired into a Printed Circuit Board (PCB). The PCB acted as the motherboard that connects the WSB to the rest of the circuit. This electrical network used two parallel voltage dividers to transform the small variations in component resistance into a measurable differential output voltage, represented in Fig. 2.

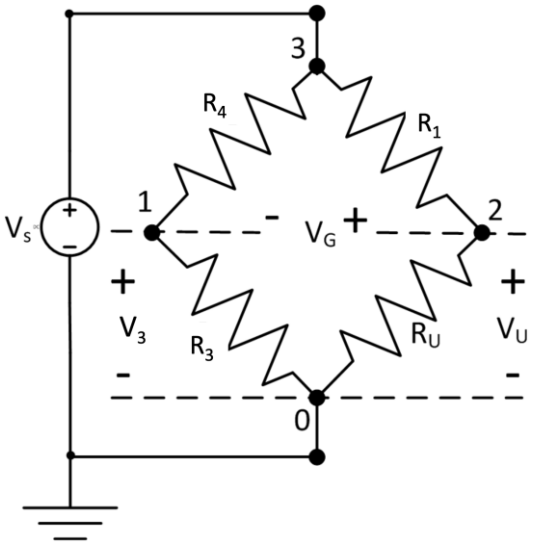

Fig. 2. Quarter Wheatstone Bridge diagram, used to understand how the circuit balances resistance values with great precision. [5].

Before converting the electronic signals into strain values, the voltage readings had to be corrected from any initial offset. A tare operation was performed to record the baseline state of

the resting circuit, yielding a fixed reference value, $V_{amp,Tare}$, for the amplified voltage (11) readings. The true change in voltage, ΔV_{amp}, caused purely by the mechanical bending of the aluminum beam was then isolated by subtracting this baseline offset from the active voltage readings, V_{amp}. This tare operation essentially zeroed out any preexisting error within the aluminum beam and strain gauge readings.

$$\Delta V_{amp} = V_{amp} - V_{amp,Tare} \tag{11}$$

To relate the measured readings of the voltage changes back to the structural properties of the beam, specific mathematical equations were applied and manipulated within the software. The fundamental relationship used to convert the recorded electrical signals into mechanical strain relied on the WSB equation (12), where V_s is the source excitation voltage, G_f is the factory-defined gauge factor of the strain gauge, ΔV_{amp} is the amplified voltage, and $gain$ represents the gained value for amplification. When considering the amplified voltage, the equation was modified to account for the inline signal scaling from the raw voltage, ΔV_g, by introducing the amplifier gain into the denominator.

$$\varepsilon = \frac{4\Delta V_{amp}}{gain V_s G_f} \tag{12}$$

The necessary components of the final equation (13) have been derived and account for each term. The equation to use for the theoretical weight was created from inserting (12) into (10).

$$W_{theory} = \frac{Ebh^2}{6L} \cdot \frac{4\Delta V_{amp}}{gain V_s G_f} \tag{13}$$

Conversely, the calibrated weight equation (14) incorporates a calibration constant, C, that is acquired experimentally using known weights, multiplied by the ΔV_{amp} value from (11). This calibrated weight measurement was used for comparison against the theoretical weight measurements.

$$W_{cal} = C\Delta V_{amp} \tag{14}$$

The calibrated weight was expected to yield a more accurate reading compared to the theoretical weight with respect to the laboratory scale with a greater certainty simply because of the calibration constant and the true change in voltage after the taring operation. These two equations (13, 14) were used in this experiment to determine the accuracy, precision, and uncertainty of both methods. Once both methods were evaluated, we were able to apply the more relevant approach to weigh the liquid container of interest, and therefore able to measure each gulp taken from the container.

The Appendix contains the full uncertainty analysis for this experiment. The uncertainties associated with the collected values, the calibration constant, C, and the final weight calculations were determined using a Monte Carlo Simulation (MCS) and Root Sum Square (RSS) propagation. This uncertainty analysis successfully modeled input variability and combined the errors to find the total uncertainty for each weight.

II. Procedure

A. Materials

The experimental setup required data acquisition hardware, circuit components, and manual measuring tools. A DAQ was necessary for collection. A USB-C to -C cable connected the DAQ to a WSB PCB to capture electrical resistance variations. Eight electrical wires were connected between the DAQ terminal ports and the bridge using a small flathead screwdriver to secure the terminal connections [10]. To construct the strain gauge-beam configuration, the strain gauge was permanently adhered to a rigid aluminum beam following the provided instructions [2]. A small hump in the wires connecting to the strain gauge was created to relieve any avoidable tension on the sensitive transducer, as seen in Fig. 3.

Fig. 3. The strain gauge was soldered to the connecting wires at the leads, and the connecting wire was taped with a hump for strain relief to avoid unnecessary stress on the sensitive wires while in use.

B. Prelab Preparations

Before collecting physical data, the digital software configuration was established. A custom virtual instrument script (VI) was built within the LabVIEW software following the configuration instructions provided [9]. This primary VI managed the incoming voltage signals from active channels to calculate weight using both methods. Within the primary program, a custom weight calculation sub-virtual instrument (sub-VI) was created to automatically process the data and ultimately served to instantly convert measured voltages into weight estimates based on the given equations mapped within the sub-VI. This was accomplished with given instructions [7]. The sub-VI within the main VI calculated the weight based on structural theory (13) while the main VI also calculated the calibrated weight simultaneously (14). Inside the LabVIEW sub-VI, the block diagram was configured with inputs for h, b, E, L, and for ε as per (10). The main VI included the Mechanics of Materials based weight estimation process but also took the ΔV_{amp} and multiplied it with a control designated as the calibration constant, or an input that a user can assign a value and was derived as per (14). Once the strain was obtained experimentally through (12), (13) was outputted from the VI.

C. Sample Window Resolution & Saturation

To optimize the signal quality before taking final measurements for weight estimation, each sample window was isolated and tested to analyze how software limitations influence digital resolution and signal saturation. The trim potentiometers for both V_g and V_{amp} were balanced near 0 V to offset any sensor baseline shifts and tared [6]. The input signal was then passed through the 14-bit ADC while individually cycling through five discrete sample windows: ±0.64 V, ±1.28 V, ±2.56 V, ±5.12 V, and ±10.24 V. The adjusted sample windows were ACH 0 and 2 as channels 1 and 3 were either unwired or unused [1]. Sample windows were selected while the beam was unloaded. Ideally, the smallest sample window size that does not saturate values would be employed. This step ensured that the final data collected would optimize signal-to-noise ratios without hitting the limits of the hardware and yield unusable data. The sample windows used were ±2.56 V and ±0.64 V for channels 0 and 2, respectively. If sample windows are too large, the resolution becomes coarse and data is not measured accurately, resulting in statistical averages and standard deviations (SD) of the data being zero. Conversely, if sample windows are too small, the mean of the dataset is typically generalized to be at or near the sample window size, indicating a saturated reading. To avoid saturation and coarse readings, sample window selection went from smallest to largest window and stopped once the mean of the dataset did not reach the limit of the sample window bounds. Following the proper selection of sample windows, the unloaded beam was tared (11) to zero any inherent offset from the resting configuration to reduce any inaccuracies.

D. Weight Estimation

With the proper sample window sizes selected and the apparatus completed, the cantilever scale was prepared for calibration. Using four known weights, they were each individually placed at roughly the same marked location on the beam. The orientation that the weights were placed in was also taken into consideration, as the known calibrating weights were not radially symmetric, and it was critical to ensure that the potential line of center of mass for the weights was perpendicular to the centerline of the beam. This cross of center lines ensured that the center of mass of each weight was placed at the same distance, L, along the beam, while being negligibly positioned slightly to the left or right of the beam's centerline.

After the data was collected for each weight, the calibration curve was created. This graph was generated by plotting the known scale weights against ΔV_{amp}, and inserting a linear line of best fit. The slope of this line was used as the calibration constant.

Having acquired the calibration constant, we were able to use the cantilever configuration as a functional scale. The choice of beverage used in this experiment was a 12-ounce bottle of Gatorade. The full bottle was first weighed using the laboratory scale to find its true weight. The bottle was then weighed 10 times at the end of the beam, as close as possible to the center mark where the calibration weights were placed. It was necessary to place the bottle, steady any vibrations or fluctuations, collect a data point, and remove the bottle from the beam completely, each time the bottle weight was measured. With this, the averages of the bottle weight were determined utilizing both methods. Each average of the measured values served as its respective full-bottle weight.

Once the full-bottle weights were obtained, incremental gulps were taken from the bottle, weighing the bottle after each gulp until the container was entirely empty. The beam was settled after each sip to minimize error in the readings. Once evacuated and consumed, the bottle was weighed using the laboratory scale to find its true empty weight.

III. Results

To begin the experiment process, the geometry for the aluminum beam and other initial values were determined for the LabVIEW software, and are presented in Table I.

TABLE I
PRIMARY DIMENSIONS & VARIABLES

Variable	Magnitude and Uncertainty
L	0.23050 ± 0.0005 m
L_0	0.28125 ± 0.0005 m
h	0.00320 ± 0.0001 m
b	0.02533 ± 0.0005 m
E	69 ± 0.1 GPa
G_f	2.0 ± 0.02
$Gain$	900 ± 4.5

The zeroing of the cantilever beam strain using the trim potentiometer and the tare operation, ΔV_{amp}, allowed us to calibrate the beam to be used as a scale. The calibrating weights of known mass were placed on a precise laboratory scale to determine their true weight. Each weight had its associated amplified voltage reading from the DAQ. The gathered values are provided in Table II.

TABLE II
SCALE CALIBRATION DATA

Scale Weight #	Mass (g)	Weight (N)*	ΔV_{amp} (V)
1	100	0.9787	0.0592 ± 0.118
2	200	1.9609	0.1434 ± 0.287
3	300	2.9395	0.2209 ± 0.442
4	400	3.9222	0.3126 ± 0.625

*Weight uncertainties with the lab scale are always ± 0.0005 N.

The information from Table II provided the basis for the acquisition of a calibration constant. Each weight and its respective amplified voltage were graphed with a line of best fit to arrive at the calibration constant necessary for a calibrated reading. The slope of the linear line yielded the calibration constant, valued at 11.695 ± 0.53 N/V (Fig. 4).

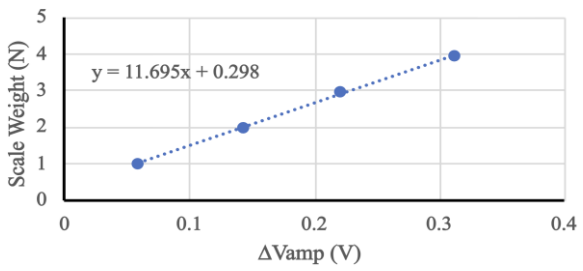

Fig. 4. Calibration curve created by plotting the scale weights versus ΔV_{amp} with an applied line of best fit to acquire the used calibration constant.

The bottle was then weighed 10 separate times on the cantilever beam where both methods were applied (Table III).

TABLE III
FULL BOTTLE WEIGHTS

W_{theory} (N)	W_{cal} (N)
3.7228 ± 0.094	3.9437 ± 0.202
3.6875 ± 0.092	3.9062 ± 0.199
3.7021 ± 0.091	3.9216 ± 0.199
3.5156 ± 0.090	3.7242 ± 0.191
3.5082 ± 0.091	3.7163 ± 0.191
3.5050 ± 0.093	3.7129 ± 0.192
3.5008 ± 0.091	3.7084 ± 0.191
3.4918 ± 0.101	3.6990 ± 0.196
3.5662 ± 0.094	3.7777 ± 0.195
3.5566 ± 0.092	3.7676 ± 0.194

The bottle was opened and its contents were slowly consumed. After each sip, the bottle was settled on the scale and weighed again, until empty. For the dataset to have optimal statistical value, it is best to try to consume the beverage in equal sips. The values of the bottle weight after each sip utilizing both methods are shown in Table IV.

TABLE IV
BOTTLE SIP WEIGHTS

W_{theory} (N)	W_{cal} (N)
2.5679 ± 0.090	2.7193 ± 0.154
1.9100 ± 0.089	2.0227 ± 0.130
1.5360 ± 0.090	1.6265 ± 0.119
1.2210 ± 0.155	1.2931 ± 0.174
0.2414 ± 0.151	0.2557 ± 0.160

The average was taken for the 10 measurements of the full bottle weight. Using this average full weight, we were able to determine how much liquid was consumed per sip based on weight using both methods, as presented in Table V.

TABLE V
SIP WEIGHT

W_{theory} (N)	W_{cal} (N)
1.0078 ± 0.128	1.0685 ± 0.254
0.6578 ± 0.127	0.6966 ± 0.202
0.3741 ± 0.127	0.3961 ± 0.177
0.3149 ± 0.179	0.3335 ± 0.211
0.9796 ± 0.216	1.0374 ± 0.236

Using the 10 samples from Table III, the mean for the full bottle weight was determined for both methods. The average theoretical weight of the full bottle was determined to be 3.5756 ± 0.066 N and the average calibrated weight of the full bottle was determined to be 3.7878 ± 0.070 N. Additionally, the mean sip weight for both methods was also determined. The average theoretical weight for each sip was determined to be 0.6668 ± 0.378 N and the average calibrated weight for each sip was determined to be 0.7064 ± 0.400 N. SD for bottle and sip weights for each method are presented in Table VI.

TABLE VI
STANDARD DEVIATIONS OF BOTTLE AND SIP WEIGHTS

σ_{theory} (Full)	σ_{cal} (Full)	σ_{theory} (Sip)	σ_{cal} (Sip)
0.0921	0.0976	0.3255	0.3450

IV. Discussion

A. Context, Objectives, & Results

The goal of this study was to assess multiple techniques for calculating the weight of a container holding liquid across varying fill volumes. These parameters affected the precision of the cantilever beam scale measurements when estimating the weight of a beverage container. By analyzing subtle changes in resistance from the strain gauge using a WSB connected to a data acquisition device, we mapped amplified voltage changes. These voltage changes can be manipulated to derive tared amplified voltages, strain, and weight values. The calculated weights and their respective uncertainties were 3.8222 ± 0.0005 N full and 0.2892 ± 0.0005 N empty (scale), 3.5756 ± 0.066 N full and 0.2414 ± 0.160 N empty (theory), and 3.7878 ± 0.070 N full and 0.2557 ± 0.151 N empty (calibrated). The calibration method ultimately yielded a highly accurate weight estimation that aligned closely with our laboratory scale reference.

B. Interpretation & Analysis

The calibrated measurement behaved as expected and yielded a much closer result with respect to the true weight compared to the theoretical measurement. Our quantitative selection of sample window sizes relied directly on optimizing signal mean and SD while maximizing resolution. Saturated readings occurred when a voltage channel hit its physical hardware limit and the signal essentially flatlines. This drove the mean to be at or near the selected sample window size and the SD to zero, but this indicated a loss of data within the LabVIEW processes and yielded inaccurate readings.

Assuming that the gauge is not a limiting factor, we were able to estimate the maximum weight that can be measured by the scale without permanently deforming the 6061-T6 aluminum beam by surpassing the yield stress ($\sigma_Y = 276\,MPa$). This is accomplished by rearranging (8) to solve for the weight and inserting the relevant variables (15).

$$W_{Max} = \frac{\sigma_Y b h^2}{6L_0} \tag{15}$$

As per Table I, and the yield stress of aluminum, σ_Y, the maximum weight without permanent deformation to the scale apparatus is 42.4 ± 0.4 N. This is well above the weight of the full beverage (3.8222 N), confirming that the beam operates entirely within the elastic regime throughout the experiment. Plastic deformation within the beam will not take place when considering the relatively light load of a single beverage. The full can exerts approximately 9.0% of the maximum allowable load, indicating plastic deformation was not a concern whatsoever. Due to (9), the strain experienced by the beam at the yield stress is approximately 0.4%, about a fifth of the maximum allowable strain from the strain gauge (2%). It is worth noting that the weight of the beam itself does not meaningfully impact the maximum load capacity and this small strain is accounted for in the tare. The zeroed strain from the weight of the beam did not affect the calibration because of the tare procedure. The weights of the full bottles were 3.8222 ± 0.0005 N for the laboratory scale, 3.5756 ± 0.066 N for the theoretical weight using Mechanics of Materials and Statics

concepts, and 3.7878 ± 0.070 N using the calibrated method. The calibration method produced a result closer to the true value, with a difference of approximately 0.0344 ± 0.070 N, while the theoretical method underestimated by approximately 0.2466 ± 0.066 N. Both methods ultimately rely on ΔV_{amp} as the input signal. However, the geometric method requires measured dimensions (b, h, L_0) and the material modulus E, each of which carried its own uncertainty. Even small errors in h, which appears cubed in the weight equation, propagate substantially into the final result. The calibration method inherently took into consideration the geometric effects into the calibration constant itself by directly mapping known weights to measured voltages, which is why it tends to agree more closely with the scale. Using the calibration method since it was more accurate, the SD for the repeatedly placed full bottle was reported as 0.0976 (Table VI). Such a low standard deviation indicated that the bottle was placed in the same location along the beam consistently. Similarly, the calibration method was chosen to analyze the weight of each sip due to the method's greater accuracy with respect to the lab scale. With the average calibrated weight of each sip being 0.7064 ± 0.400 N, the SD for this sample was 0.3450 (Table VI). This standard deviation is greater than that of the repeated calibrated weight of the full bottle. The variation in gulp size is expected given that taking perfectly consistent sips of liquid by volume is difficult to achieve without mechanical assistance such as a syringe. The SD of the gulp sizes captures human variability. The weights of the empty bottles were 0.2892 ± 0.0005 N for the laboratory scale, 0.2414 ± 0.160 N for the theoretical weight using Mechanics of Materials and Statics concepts, and 0.2557 ± 0.151 N using the calibrated method. Once again, the calibration method produced a result closer to the true value, with a difference of approximately 0.0335 ± 0.151 N, while the theoretical method underestimated by approximately 0.0478 ± 0.160 N.

C. *Uncertainty & Limitations*

Uncertainty in both weight estimates, final full and empty weights for theoretical and calibrated methods, was propagated using RSS analysis, combining all contributing variable uncertainties. It is worth noting that in all aspects of this laboratory experiment, no measurement obtained is truly exact. Numerical values that were obtained inherently have uncertainty that reflects a range for the potential true value of the measurement. For the calibrated method (14), the uncertainty of the calibration constant, C, was determined using MCS and the uncertainty of ΔV_{amp} was determined using RSS propagation from statistical uncertainties in V_{amp} from the 2500 samples from the DAQ having considered the 95% confidence interval. For the method that relied on theory, uncertainty is propagated through each variable in (13). Though statistical uncertainties were determined using the 95% confidence interval, the uncertainty analysis was calculated considering RSS propagation. Though the propagated uncertainties for the full bottle weights using both methods was determined, the SD for the dataset was 0.0976 (calibrated), showing that the bottles were placed relatively close to one another, and that fluctuations in the bottle placement were minimal. Since the variability in placement was so miniscule and borderline negligible, it was determined that repeatability of bottle placement was not an issue for uncertainty considerations. A low SD corresponds to a low uncertainty for the bottle weights in the 10 repeated placements, demonstrating a low contribution to final uncertainty when propagated. A student's t-distribution was used because of the small sample size, $n = 10$. With degrees of freedom (df), $df = n - 1$, a t value of 2.262 was used to conduct statistical analysis of the dataset. Several modifications could improve the accuracy and precision of the instrumented cantilever beam scale. Integrating a higher-bit ADC would help push step-size resolution limitations and exponentially decrease the uncertainty. The collection of more data can also yield more precise results that can be interpreted considering the 95% confidence interval, aiding with the determination of accuracy and the meaning of uncertainty. Implementing a physical barrier to ensure that calibration weights are placed in the same location, reducing uncertainty in the calibration constant. This concept should also be applied to the beverage of choice when weighing it 10 times, as it would further reduce placement variability, though this has already been shown to be a minor contributor. Additionally, using a longer beam would increase the bending moment from a load. A larger moment corresponded to a larger ΔV_{amp}, being especially considerable for low-strain applications such as the empty bottle. Lastly, since the height, h, of the beam is cubed, its error is propagated strongly throughout the uncertainty analysis, making it the largest contributor to uncertainty. To accurately measure the height of the beam would yield significantly more accurate results and consequently produce a lower uncertainty.

V. Conclusion

This experiment successfully demonstrated the use of a strain gauge as a transducer to estimate the weight of a beverage at varying levels of fill. This was done by measuring microscopic voltage fluctuations from a cantilevered 6061-T6 aluminum beam and transforming those values into measurable strains, from which applied load was computed through two independent methods. Using beam theory from Mechanics of Materials, the full can was estimated to weigh 3.5756 ± 0.066 N, and the empty can 0.2414 ± 0.160 N. Using the calibration constant method, the full and empty can weights were estimated to be 3.7878 ± 0.070 N and 0.2557 ± 0.151 N, respectively, against lab scale readings of 3.8222 ± 0.0005 N and 0.2892 ± 0.0005 N. These results demonstrate the viability of strain-based weight estimation and the potential value this instrumentation approach can bring to fields requiring dynamic, non-invasive load measurement.

Appendix

A. *Cantilever Beam Dimension Uncertainties*

The uncertainty for the geometry of the aluminum beam and other initial values was determined. The following values in Table VII were provided by the manufacturer or acquired by rule of thumb [3, 8]. These values were necessary as the basis for the later calculated RSS propagated uncertainty in the final

weights for the calibration constant method and the Mechanics of Materials/Statics method.

TABLE VII
BEAM VARIABLES & UNCERTAINTIES

Variable	Symbol	Uncertainty	Source
L	μ_L	± 0.0005 m	Manufacturer [3]
L_0	μ_{L_0}	± 0.0005 m	Manufacturer [3]
h	μ_h	± 0.0005 m	Manufacturer [3]
b	μ_b	± 0.0001 m	Rule of Thumb [8]
E	μ_E	± 0.1 GPa	Rule of Thumb [8]
G_f	μ_{G_f}	± 0.02	Manufacturer [8]
$Gain$	μ_{Gain}	± 4.5	Manufacturer [3]
W_{True}	$\mu_{W_{True}}$	± 0.0005 N	Manufacturer [3]

B. Statistical Uncertainties

Statistical uncertainties relied on the 95% confidence interval from the 2500 collected samples from LabVIEW. This allowed the standard deviation to be multiplied by 2 to obtain the statistical uncertainty of the direct measurements from the LabVIEW software outputted data. Table VIII provides the directly-measured 10 V_{amp} values and their respective uncertainty for the full bottle weights.

TABLE VIII
FULL BOTTLE WEIGHTS V_{amp} & UNCERTAINTY

V_{amp} (V)	Uncertainty (V)
0.30934	± 0.0082
0.30614	± 0.0080
0.30745	± 0.0079
0.29057	± 0.0078
0.28990	± 0.0079
0.28960	± 0.0081
0.28922	± 0.0079
0.28841	± 0.0089
0.29515	± 0.0082
0.29428	± 0.0080

Similarly, Table IX provides the directly-measured 5 V_{amp} values and their respective uncertainties for the bottle weights after each sip.

TABLE IX
BOTTLE SIP WEIGHTS V_{amp} & UNCERTAINTY

V_{amp} (V)	Uncertainty (V)
0.20393	± 0.0080
0.14437	± 0.0080
0.11050	± 0.0081
0.08198	± 0.0140
0.00672	± 0.0136

The final statistical uncertainty is from the Monte Carlo Simulation. This simulation required the weights of each calibration weight, its respective ΔV_{amp}, and the uncertainties for each value. Monte Carlo Simulation works by taking the known plus-minus range of the given values and generates thousands of randomized trials to create a statistically sound dataset that satisfies the 95% confidence interval. This maps the range of possibilities of values that are likely to occur. The Monte Carlo Simulation used for this experiment was specifically a four-point MCS due to the four calibration weights used. Ideally, the simulation would run as many variations as possible to completely capture the full range of possibilities. The results of the MCS are shown in Table X.

TABLE X
MONTE CARLO SIMULATION VALUES

Variable	Value	Uncertainty
W_{Cal_1}	0.9787 N	± 0.0005 N
W_{Cal_2}	1.9609 N	± 0.0005 N
W_{Cal_3}	2.9395 N	± 0.0005 N
W_{Cal_4}	3.9222 N	± 0.0005 N
ΔV_{amp_1}	0.05916 V	± 0.0081 V
ΔV_{amp_2}	0.14345 V	± 0.0106 V
ΔV_{amp_3}	0.22087 V	± 0.0121 V
ΔV_{amp_4}	0.31264 V	± 0.0079 V
C	11.695 N/V	± 0.53 N/V

C. RSS Uncertainties

The following values had to be acquired through RSS uncertainty propagation because they were used in calculation for the experiment. Table XI provides the uncertainty values for ΔV_{amp}, W_{theory}, and W_{cal} for the repeated weighing procedure of the full bottle.

TABLE XI
FULL BOTTLE UNCERTAINTIES

$\mu_{\Delta V_{amp}}$ (V)	$\mu_{W_{theory}}$ (N)	$\mu_{W_{cal}}$ (N)
± 0.010	± 0.094	± 0.202
± 0.014	± 0.092	± 0.199
± 0.013	± 0.091	± 0.199
± 0.011	± 0.090	± 0.191
± 0.015	± 0.091	± 0.191
± 0.022	± 0.093	± 0.192
± 0.009	± 0.091	± 0.191
± 0.010	± 0.101	± 0.196
± 0.012	± 0.094	± 0.195
± 0.019	± 0.092	± 0.194

Similarly, Table XII provides the uncertainty values for ΔV_{amp}, W_{theory}, and W_{cal} for the bottle weight after each sip.

TABLE XII
BOTTLE SIP UNCERTAINTIES

$\mu_{\Delta V_{amp}}$ (V)	$\mu_{W_{theory}}$ (N)	$\mu_{W_{cal}}$ (N)
± 0.024	± 0.090	± 0.154
± 0.023	± 0.089	± 0.130
± 0.011	± 0.090	± 0.119
± 0.016	± 0.155	± 0.174
± 0.028	± 0.151	± 0.160

With the RSS propagated through each equation, the final results of the weights and their uncertainties were determined and are provided in Table XIII.

TABLE XIII
FINAL WEIGHTS RESULTS

Technique	Full (N)	Empty (N)
Scale	3.8222 ± 0.0005	0.2892 ± 0.0005
Theory	3.5756 ± 0.066	0.2414 ± 0.160
Calibration	3.7878 ± 0.070	0.2557 ± 0.151

For RSS propagated uncertainties, the differential voltage (11) uncertainty was taken into consideration when using the measured voltages and tare voltage values (16).

$$\mu_{\Delta V_{amp}}^2 = \left(\frac{\partial \Delta V_{amp}}{\partial V_{amp}}\mu_{V_{amp}}\right)^2 + \left(\frac{\partial \mu_{\Delta V_{amp}}}{\partial \mu_{V_{amp},Tare}}\mu_{V_{amp,Tare}}\right)^2 \quad (16)$$

The uncertainty of the strain, ε, was then determined for (12) using RSS propagation (17).

$$\mu_\varepsilon^2 = \left(\frac{\partial \varepsilon}{\partial V_s}\mu_{V_s}\right)^2 + \left(\frac{\partial \varepsilon}{\partial G_f}\mu_\varepsilon\right)^2 + \left(\frac{\partial \varepsilon}{\partial gain}\mu_{gain}\right)^2 + \left(\frac{\partial \varepsilon}{\partial \Delta V_{amp}}\mu_{\Delta V_{amp}}\right)^2 \quad (17)$$

After the stain, the uncertainty of the stress, σ, was then determined for (9) using RSS propagation (18).

$$\mu_\sigma^2 = \left(\frac{\partial \sigma}{\partial E}\mu_E\right)^2 + \left(\frac{\partial \sigma}{\partial \varepsilon}\mu_\varepsilon\right)^2 \quad (18)$$

Lastly, the RSS propagated weights for both methods, theoretical (13) and calibrated (14), was determined (19, 20).

$$\mu_{W_{theory}}^2 = \left(\frac{\partial W_{theory}}{\partial h}\mu_h\right)^2 + \left(\frac{\partial W_{theory}}{\partial b}\mu_b\right)^2 + \left(\frac{\partial W_{theory}}{\partial L}\mu_L\right)^2 + \left(\frac{\partial W_{theory}}{\partial E}\mu_E\right)^2 + \left(\frac{\partial W_{theory}}{\partial \varepsilon}\mu_\varepsilon\right) \quad (19)$$

$$\mu_{W_{cal}}^2 = \left(\frac{\partial W_{cal}}{\partial C}\mu_C\right)^2 + \left(\frac{\partial W_{cal}}{\partial \Delta V_{amp}}\mu_{\Delta V_{amp}}\right)^2 \quad (20)$$

REFERENCES

[1] S. Ridgeway, “EML 3301C Cantilever Beam Scale”, Gainesville, FL: 2026, unpublished.
[2] S. Ridgeway, “EML 3301C Quarter Bridge Strain Gage Mounting Steps”, Gainesville, FL: 2026, unpublished.
[3] S. Ridgeway, “Lab 2”, Gainesville, FL: 2026, unpublished.
[4] S. Ridgeway, “Lab 2 Discussion”, Gainesville, FL: 2026, unpublished.
[5] S. Ridgeway, “Lab 2 Intro_Strain Gage_Wheatstone Bridge”, Gainesville, FL: 2026, unpublished.
[6] S. Ridgeway, “Lab 2 Procedure”, Gainesville, FL: 2026, unpublished.
[7] S. Ridgeway, “Lab 2 subVI”, Gainesville, FL: 2026, unpublished.
[8] S. Ridgeway, “Lab 2 Uncertainty”, Gainesville, FL: 2026, unpublished.
[9] S. Ridgeway, “Lab2 VI”, Gainesville, FL: 2026, unpublished.
[10] S. Ridgeway, “Wheatstone Bridge Construction”, Gainesville, FL: 2026, unpublished.